Conceptual design of a radial collimator for MIRACLES, the time-of-flight backscattering spectrometer at the European Spallation Source

Roberto Martínez,[1*] *Marton* Marko,[2] *Alexander* Conde,[1] *Aitor* Zugazaga,[1] *Idoia* Mazkiaran,[1] *Octavio* G. del Moral,[1] *Giles* Harper,[1] *José E.M.* Pereira,[1] *Heloisa* N. Bordallo,[3,4] and *Félix* J. Villacorta[1]

[1]ESS-Bilbao. Parque Científico y Tecnológico Bizkaia Nave 201, 48170 Zamudio, Spain
[2]Neutron Spectroscopy Department, Wigner Research Centre for Physics, Konkoly Th. M. 29-33, 1122 Budapest, Hungary
[3]Niels Bohr Institute-University of Copenhagen. Universitetsparken 5 -2100 Copenhagen, Denmark
[4]ESS ERIC, P.O. Box 176, SE-22100 Lund, Sweden

Abstract. A parametrized conceptual design for a radial collimator in a neutron backscattering instrument is presented, with application to the characteristic geometry of the MIRACLES spectrometer, that will be constructed at the European Spallation Source (ESS). The analytic development of this design has considered both the forward scattering (sample-analyzer) and backscattering (analyzer-detectors) pathways. All the characteristic dimensions (internal and external radii, slit angle) and figures of merit (such as transmission and estimated background reduction) of the device are calculated as a function of the focal points. Finally, the estimated performance of the final concept has been validated by Monte Carlo simulations.

1 Introduction

An essential aspect in the design of any neutron spectrometer is the optimization of the signal-to-background ratio, that is, the minimization of neutrons scattered from sample environment equipment or from any in-vessel component that could arrive at the detectors and degrade the quality of the spectra. This is especially critical in indirect-geometry spectrometers in neutron time-of-flight instruments, that feature a significant flux at the sample due to their large-bandwidth [1,2]. These neutrons can scatter (Bragg, incoherent…) with devices around the sample environment, and can contribute negatively to the correct performance of the experiments.

Radial collimators are the elements whose aim is to block radiation sourced from these background-generating regions [3–5]. From the first radial collimators, developed at the ILL (Institut Laue-Langevin, Grenoble, France) [6], a number of neutron instruments included a radial oscillating collimator (ROC) − with low oscillation periods of the order of the ~10 s − as a valuable component to further improve the background ratio [7].

This work reports on the conceptual design of a radial oscillating collimator for MIRACLES, the time-of-flight backscattering spectrometer at the European Spallation Source [8,9]. Most published concepts on radial collimators are related to diffractometers [10,11] or direct-geometry spectrometers [7,12]. This work has extended the design considerations towards backscattering spectrometers. Along the process, the main variables (inner and outer radii, slit size…) have been parametrized to offer a solution that can be adapted to changes in the design of the secondary spectrometer. The final parameters for MIRACLES are based on the specificity of the geometry of the secondary spectrometer; in particular, the detector bank layout has defined the slit size and the inner radius of the radial collimator. Finally, the estimated performance has been validated by Monte Carlo simulations.

2 Material and methods

The analytical calculations have been carried out for both scattering and backscattering flightpaths. Intuitively, the radial oscillating collimator provides a better functionality by placing it close to the detectors, to suppress neutrons stemming from spurious scattering in the backscattering pathway (Fig. 1a). This collimator is oscillating, aiming to average the shadowing effect provided by the blades to the nearby detectors. Thus, the oscillation range is set to be of the order of the angular coverage of a detector tube. In order to reach this averaging effect, the oscillation period of the collimator should be both slower than the ESS pulse period (71.4 *ms*) but faster than the measurement time (~30 – 60 *min*). However, all calculations in this paper have been carried out for a collimator in a static state, without loss of generality of the final results for an oscillating case.

Moreover, if the collimator simply accounts for one only pathway, either the sample-analyzer or the

* Corresponding author: rmartinez@essbilbao.org

backscattering analyzer-detector pathway, some undesirable shadowing issues due to the mechanical frame can reduce the angular acceptance of the instrument (for MIRACLES the angular coverage is 9.5 to 165° in the horizontal, and ±22° in the vertical). Thus, for a backscattering spectrometer, neutrons must go through the collimator channels twice, in the scattering and the backscattering pathways (Fig. 1a).

The radial collimator considers the following parameters (see also Fig. 1b):

- X-axis: scattering axis (direction of the scattered beam).
- Y-axis: perpendicular to X-axis, in the same scattering plane (equatorial).
- 2θ: scattering angle (angle incoming beam – scattered beam).
- r_m: inner radius of the collimator.
- R_M: outer radius of the collimator (channel/blade length: R_M - r_m).
- ϕ: angle between blades (slit size).
- $2d$: width of a blade (a constant thickness blade [5] is assumed).
- $2F_y$: focal width (sight of a slit at the sample position).
- d_s: sample size (cylinder diameter).
- R_d: radius of the detector array.

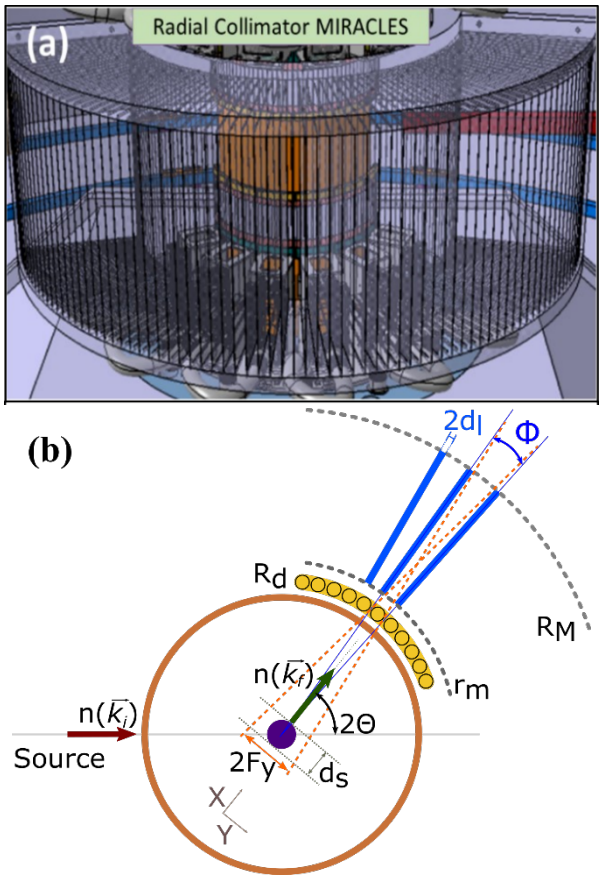

Fig. 1. (a) 3D preliminary model of the MIRACLES radial collimator; (b) Geometry of the radial collimator calculations.

The main parameters needed to design a radial collimator (signal transmission, T, background reduction, R) will be parametrized as a function of the collimator characteristics and the sample size (ϕ, r_m, R_M, d_s). The estimated performance has been validated by Monte Carlo neutron optics calculations using the McStas [13] available components (in particular, *Exact_radial_coll* is used to simulate the physical radial collimator. Finally, analytical calculations of the neutron absorbing layer used to coat the collimator blades were corroborated by simple MCNP calculations.

3 Results and discussion

3.1 General model

Let us focus our attention on one slit of the ROC. The concept behind the design efforts resides in the characterization of any possible radial collimator by defining two focal lines that describe the extreme neutron paths transmitted by a slit of the collimator (orange dash lines in Fig. 2). These lines define in turn two focal lengths: a focal abscissa F_x that marks the crossing between the two focal lines along the X-axis, and a focal ordinate F_y which defines the distance between the crossing points of the focal line with the Y-axis, located at the sample position (Fig. 2). With this layout, the range $(-F_y, +F_y)$ of length $2F_y$ defines the focal width. This focal width includes not only the sample (cylinder of diameter d_s) but also the area around it (sample environment). Any neutron scattered by any point y_s within this range in the Y-axis is transmitted through the collimator slit if the scattering angle is limited by the angle between the focal lines, β. Additionally, the intersection points between focal lines, F_x, is related to the inner and outer radii for each possible radial collimator (r_m and R_M respectively).

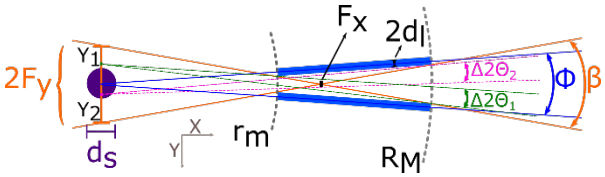

Fig. 2. Sight of the sample area by a single slit (blue radial blades) showing the main parameters defining the radial collimator: focal lines (orange), focal lengths F_x and F_y, slit aperture angles Φ and β, inner (r_m) and outer radius (R_M), blade length (or collimation length, R_M - r_m) and blade width ($2d_l$).

Thus, let y_s be scattering points within the $(-F_y, +F_y)$ range that scatters neutrons through a slit of the collimator (see Fig. 2). Assuming a slit periodicity of ϕ, and approaching to small angles, the actual angular acceptance of a slit for the radial collimator (transmittance divergence) is $\Delta 2\theta$, that ranges from $\Delta 2\theta = 0$ (for the focal lines, starting at points $\pm F_y$) to $\Delta 2\theta = \phi$ (for a central point sample, at $y = 0$). Two different points, y_1 and y_2, representing scattering points of the sample environment and the sample, respectively (Fig. 2), deliver neutrons inside a collimator channel (slit) with divergence $\Delta 2\theta_1$ and $\Delta 2\theta_2$ (represented by green and pink dash lines, respectively). This divergence $\Delta 2\theta$ are delimited by angles $2\theta_+$ and $2\theta_-$:

$$2\theta_+ = 2\theta_0 + \frac{\phi}{2} - \frac{(y + d_l)}{r_m} \quad (1)$$

$$2\theta_- = 2\theta_0 - \frac{\phi}{2} - \frac{(y - d_l)}{R_M} \quad (2)$$

$$\begin{aligned} \Delta 2\theta(y) &= 2\theta_+ - 2\theta_- \\ &= \phi - y\left(\frac{1}{r_m} - \frac{1}{R_M}\right) \\ &\quad - d_l\left(\frac{1}{r_m} + \frac{1}{R_M}\right) \end{aligned} \quad (3)$$

This general expression, that displays the finite sample size and the finite blade effects, results in $\Delta 2\theta = \phi$ in the ideal case of a point sample ($y = 0$) and zero blade thickness ($d_l = 0$).

As previously mentioned, focal lines (scattering trajectories starting at points $\pm F_Y$ display a transmitted divergence is $\Delta 2\theta = 0$:

$$\begin{aligned} \Delta 2\theta(F_Y) &= \phi - F_Y\left(\frac{1}{r_m} - \frac{1}{R_M}\right) \\ &\quad - d_l\left(\frac{1}{r_m} + \frac{1}{R_M}\right) = 0 \end{aligned} \quad (4)$$

From here, two characteristic radii r_c and r_c' can be defined as:

$$r_c' \cong \left(\frac{1}{r_m} + \frac{1}{R_M}\right)^{-1} \quad (5)$$

$$r_c \cong \left(\frac{1}{r_m} - \frac{1}{R_M}\right)^{-1} \quad (6)$$

Then, from eq. (4):

$$F_Y = \left(\phi - \frac{d_l}{r_c'}\right) r_c \quad (7)$$

Since d_l is typically small (~0.1 mm, thus $d_l \ll r_m$, R_M), there is a direct relationship between the slit size and the observable focal width around the sample, in agreement with previous results [4,5,10]:

$$F_Y \cong \phi r_c \quad (8)$$

The focal abscissa F_X is also related to the parameters of the collimator. The angle delimited by the focal lines, β, can be linked to the inner and outer radius:

$$\tan\frac{\beta}{2} = \frac{r_m \tan\left(\phi/2\right)}{F_X - r_m} = \frac{R_M \tan\left(\phi/2\right)}{R_M - F_X} \quad (9)$$

This second term in (9) results in an expression for F_X:

$$F_X = 2r_c' \quad (10)$$

Somehow, the location of the focal lines and their characteristic focal point F_X and focal width F_Y can reveal at first glance the angular acceptance, and the slit dimensions (angle ϕ and radii r_m *and* R_M, see Fig. 3 for variable F_X and fixed $2F_Y$ =30 mm).

3.2 Transmission

The transmitted neutrons are estimated using the transmission quality factor T, defined as the ratio between the number of neutrons scattered from the sample at the exit of a collimator slit and the number of neutrons at its entrance ($T = \frac{I_t}{I_i}$).

A relationship (q ratio) can be established between the sample size, d_S, and the focal width, $2F_Y$:

$$q = \frac{d_S}{2F_Y} \quad (11)$$

where $0 < q < 1$. In the case where q=1 the sample region would completely lie inside the focal width of the slit and $d_S = 2F_Y$.

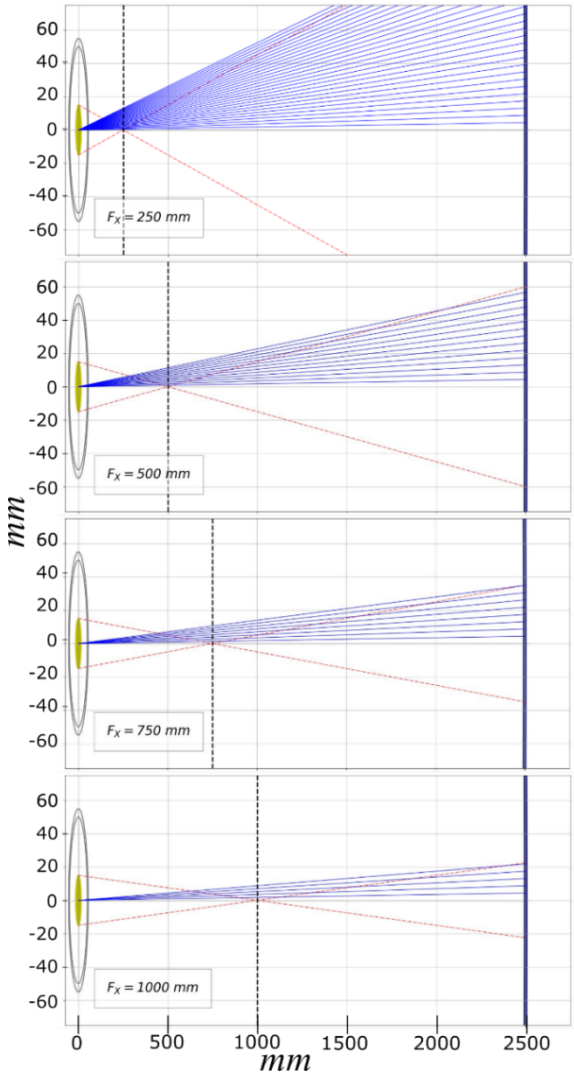

Fig. 3. Different slit configurations for fixed $2F_Y$ =30 *mm* and variable F_X from 250 to 1000 *mm*. The solutions for r_m and R_M radii are the intersections of the radial blue lines (having an angle ϕ) with the red-dashed focal lines.

Considering neutrons scattered by the sample, the total intensity, I_t, at the entrance of the slit is related to the angle distribution (aperture), ϕ:

$$I_i = \int_{-\frac{d_S}{2}}^{\frac{d_S}{2}} \phi(y)dy = 2\int_0^{\frac{d_S}{2}} \phi(y)dy = \\ = 2\int_0^{qF_Y} \phi(y)dy = \\ = 2qF_Y{}^2 r_c^{-1} \quad (12)$$

The total intensity at the exit (transmitted) from one channel is the integral of the total transmittance divergence stated in Eq. (3) along the sample along the Y-axis:

$$I_t = \int_{-\frac{d_S}{2}}^{\frac{d_S}{2}} \Delta 2\theta(y)dy = 2\int_0^{\frac{d_S}{2}} \Delta 2\theta(y)dy \\ = 2\int_0^{qF_Y} \Delta 2\theta(y)dy \quad (13)$$

Assuming that $d_s \ll r_m$, R_M:

$$I_t = 2\int_0^{qF_Y} \phi(y)dy - 2\int_0^{qF_Y} yr_c^{-1}dy \\ = I_i - 2\int_0^{qF_Y} yr_c^{-1}dy \\ = I_i - (qF_Y)^2 r_c^{-1} \quad (14)$$

The transmission parameter of a slit belonging to the radial collimator is then:

$$T = \frac{I_t}{I_i} = 1 - \frac{(qF_Y)^2 r_c^{-1}}{2qF_Y{}^2 r_c^{-1}} = 1 - \frac{q}{2} \quad (15)$$

Thus, in the common case that $d_s \ll r_m$, R_M, the transmission depends on the ratio q between the sample size and the focus size. Retrieving the expression for the ROC parameters ($2F_Y$, ϕ, r_m, R_M) and the sample size, d_s:

$$T = 1 - \frac{d_S}{4F_Y} = 1 - \frac{d_S}{4\phi r_c} \quad (16)$$

3.3 Background reduction

Background neutrons come mainly from spurious and not controlled scattering with in-vessel components. This randomness renders a challenging observation of the background reduction functionality and performance of the component. However, a qualitative estimation can be attempted, using sample environment equipment as a primary source of background.

On one note, the sample environment can be simplified to a hollow cylindrical model with radius R_{SE}, (a circumference in the sample plane with length $2\pi R_{SE}$).

Furthermore, the number of neutrons scattered by the sample environment and transmitted through the slit is proportional to the arc lengths in the direct line of sight of the sample by the slit, Δl, which is always $4F_Y$ (see Figure 4, being $\Delta l = 2d_s$ when $d_s = 2F_Y$, i.e., when q=1, thus T = ½).

Thus, for a hollow cylindrical sample environment equipment, the background reduction can be defined as the ratio between the number of neutrons scattered by the sample environment and transmitted through the slits (background after implementation of the ROC, B_{coll}) with respect to the total number of neutrons scattered by the sample environment (background without using the collimator, B_0):

$$R = \frac{B_{coll}}{B_0}T = \frac{\Delta l}{2\pi R_{SE}}T \approx \frac{2F_Y}{\pi R_{SE}}T \quad (17)$$

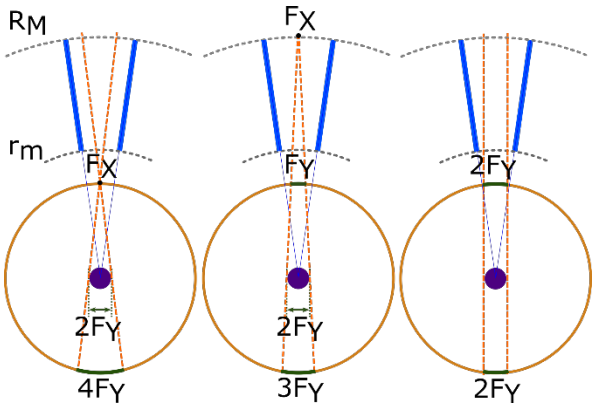

Fig. 4. Representation of the amount of sample environment region (orange circle) "observed" by the slit (green arcs) for three extreme cases of blade configuration corresponding to focal lenghts F_X lying either before r_m (left), between R_M and r_m (center), or beyond R_M (right). For each case the arcs observed by the slit can be effectively approximated to ~$4F_Y$.

3.4 Backscattering pathway

The background is minimized largely in the sample-analyzer pathway. Neutrons scattered from a sample passing through a collimation channel (slit) will reach a segment (see Fig. 5a) of the analyzer given by:

$$A_A = 2R_A \sin\frac{\phi}{2} \quad (18)$$

Recalling the description of Figure 2 for focal lines, the total projection of neutrons passing through a slit to the analyzer has a length, P_A, that covers an angle β ($\tan\beta = \frac{r_c}{r_c'}\tan\phi$, see Fig. 5a), where:

$$\frac{F_Y}{F_X} = \tan{}^{\beta}/_{2} = \frac{{}^{P_A}/_{2}}{R_A - F_X} \quad (19)$$

$$P_A = 2F_y\left(\frac{R_A}{F_X} - 1\right) \quad (20)$$

The backscattering trajectory, after reflection from the analyzer, follows a trajectory distribution centered at the same slit. There is a possibility some neutrons arrive not at the corresponding ^{3}He tube detector, but in the adjacent ones (see inset of Figure 5b), since the collimator is not in contact with the detector array ($r_m > R_A$). The arc of the detector array circumference where the neutrons from a determined slit impact (it can be called "detector impact arc", a_m) is defined by the slit aperture for the minor radius:

$$a_m = 2r_m \sin\frac{\phi}{2} \quad (21)$$

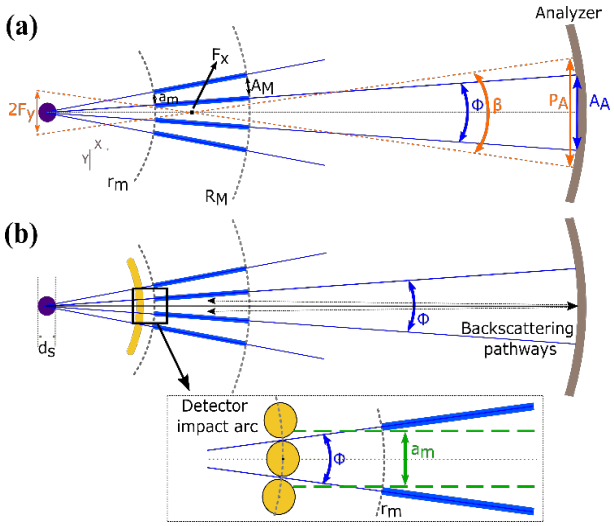

Fig. 5. (a) Schematic representation of forward scattered neutrons passing through a single slit of the collimator and arriving to the analyzer. (b) Schematic representation of backscattered neutrons arriving to the detector array (green dashed lines) define the *detector impact arc* a_m.

3.5 Application to MIRACLES

The previous general method has been conceived to generate all the possible radial collimator configurations. Nevertheless, constraints imposed by realistic design of the MIRACLES secondary spectrometer eventually determine the final parameters. For instance, the slit angle ϕ is determined by the angular sector covered by the detector tubes: since the detector banks for MIRACLES are cylindrical arrays with radius R_d = 230 *mm*, and tubes have 12.8 *mm* diameter, the repetition angle is $\phi = 3.24°$.

Additionally, the inner radius, r_m, should be placed as close as possible to the detectors, to optimize the dimensions of the collimator, and minimize the arrival of neutrons to adjacent detector tubes. Considering the detector frame and other spatial considerations, the minimum value is r_m = 300 mm. Finally, MIRACLES is designed to measure sample sizes of 30 *x* 30 mm^2 (thus, d_s = 30 *mm*), and by default, the radius of any sample environment equipment used in MIRACLES shall be smaller than the sample chamber radius, thus $R_{SE} \leq 210$ *mm*).

A key factor is that the focal width, $2F_y$, can be larger than the sample size, d_s; however, to minimize the inclusion of sample environment equipment such $2F_y$ parameter should be as close as possible to the sample bore, the small vessel that hosts the sample inside the SE equipment. In an orange cryostat, this bore size is around 50 - 70 *mm*, and some small magnets show a sample space of 80 *mm*. Thus, selecting a $2F_y$ of about this size minimizes the transmission of neutrons scattered by the SE equipment, beyond the sample bore walls.

Table 1 shows results of different radial collimator options as a function of selected focal widths, $2F_y$, and the inner radii, r_m. The transmission *T* has been compared in some examples with the transmission obtained after Monte Carlo calculations (using McStas, see also Figs. 6a and 6b), providing a good match between them (with an underestimation of the first with respect to the latter within 10%). For the background reduction figure of merit, *R*, the sample environment radius has been fixed to R_{SE} = 210 *mm*.

Assuming an analyzer radius of R_A = 2500 *mm*, a detector array radius of R_d = 230 *mm*, and a radius of the ½-inch detector tubes of r_d = 6.35 *mm*, the view (spot) of a slit on the analyzer is:

$$A_A = 2R_A \sin\frac{\phi}{2} = 141\ mm \qquad (22)$$

Finally, Fig. 6c shows the dependence of the collimation length (also called blade length, $R_M - r_m$) on the focal width, $2F_y$, and the inner radius, r_m. It is intuitive to

Table 1. A list of potential options for the MIRACLES radial collimator and estimated performance in terms of transmission (comparing analytical and Monte Carlo calculations), background reduction, and detector impact.

r_m (mm)	R_M (mm)	$2F_y$ (mm)	*T*	*T* (MC)	*R*	a_m (mm)	$a_m/2r_d$ (# tubes)
300	582	70.0	0.79	-	0.083	17	1.3
300	599	68.0	0.78	0.84	0.080	17	1.3
300	690	60.0	0.75	0.82	0.068	17	1.3
300	935	50.0	0.70	0.77	0.053	17	1.3
330	707	70.0	0.79	-	0.083	18.6	1.5
350	805	70.0	0.79	-	0.083	19.8	1.6
350	693	80.0	0.81	0.86	0.098	19.8	1.6
400	920	80.0	0.81	0.85	0.099	22.6	1.8

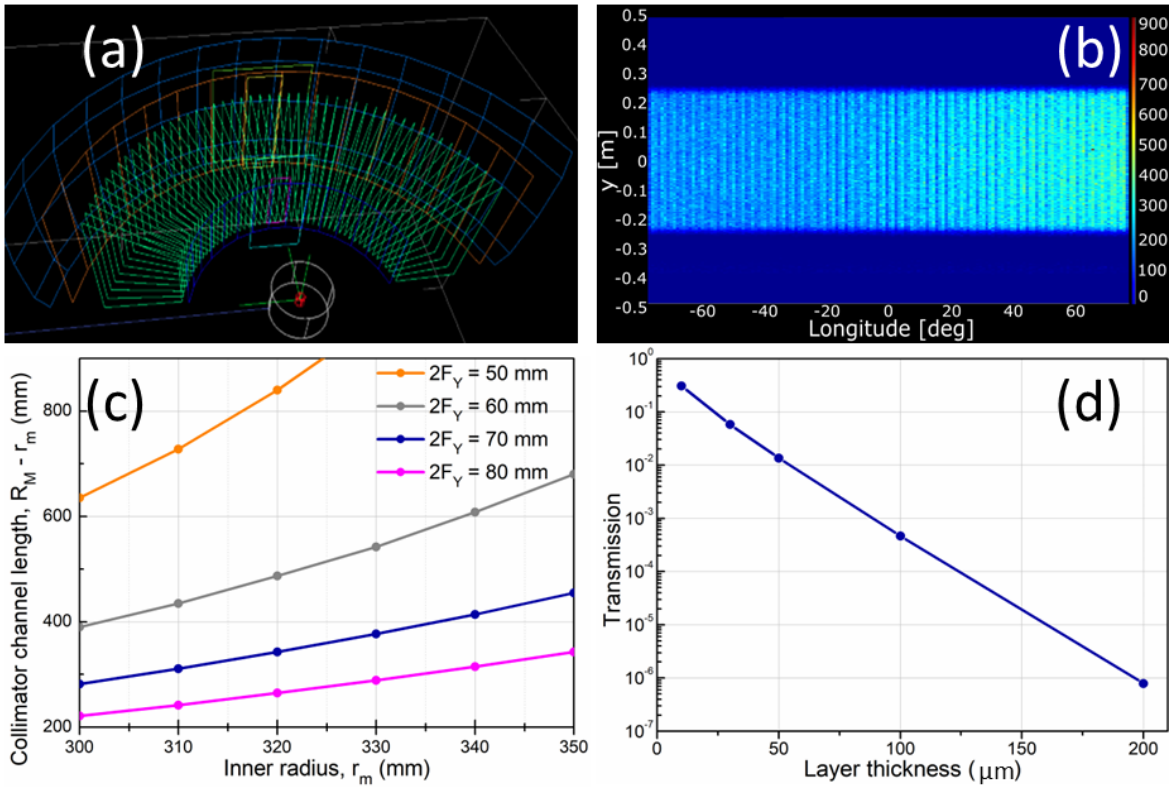

Fig. 6. (a) McStas visualization of the radial collimator for MIRACLES (b) Signal collected by a McStas position sensitive monitor at the exit of the collimator in the forward scattering (c) Collimation length (that can serve or relative comparison of ROC dimensions and cost) as a function of the inner radius and focal length; (d) Thermal neutron absorption factor (1/attenuation factor) of a Gd_2O_3 layer as a function of the layer thickness, obtained by MCNP.

deduce that this collimation length is directly related with the final cost of the ROC. Results show that, on one hand, in order to cover the same focal width (determined by the sample bore), the closest the collimator is to the detector bank ($r_m \rightarrow R_d$), the shorter the collimation length required. On the other hand, it is observed that to reach smaller focal widths (for smaller sample bore dimensions), the collimation lengths need to be longer, for a given value of r_m.

From all the potential results, the best option consists of reaching the closest position possible of the collimator with respect to the detectors bank (r_m = 300 *mm*) and, assuming a sample bore size of the sample environment equipment (e.g., MIRACLES cryostat) of 70 *mm*, fixing a focal width that reduces 1 *mm* at each side of the sample bore, (i.e., $2F_Y$ = 68 *mm*). With these parameters an external radius of R_M = 599 *mm*, is obtained, with a transmission estimated of about ~80%, and a detector impact arc of $a_m/2r_d$=1.3 detectors.

3.6 Thickness of the blade shielding

The collimating blades, typically made of thin aluminum, PETP or Kapton sheets of thickness ~100 *mm*, less than 1% of the channel width, are coated with a neutron capturing layer, usually Gd_2O_3 paint. An estimation of the minimum thickness of this coating, t, has been carried out, considering that the blade transmission can be calculated as $\tau = e^{-N\sigma t}$, where $N = N_A\rho/M$ is the molecular density of Gd_2O_3 (N_A is the Avogadro number, M = 362.5 *g/mol* is the molecular weight and ρ is the density: 7.407 g/cm^3) and $\sigma = 5 \times 10^{-20}$ $cm^2/atom$ is the cross section of natural Gd at thermal neutrons with E = 25 *meV*.

Aiming at an attenuation factor of ~10^{-3}, ($\tau = 10^{-3}$) and assuming that density is reduced by ½ to simulate that the paint is Gd_2O_3 powder mixed in epoxy, the minimum layer thickness required is ~360 μm (180 μm on each side of the blade). This estimation is corroborated by simple Monte Carlo calculations (see Fig. 6d). The maximum grazing incidence angle, ξ, that a neutron scattered by sample environment equipment with radius R_{SE} = 210 *mm* can have crossing a single blade (that is, higher angles will convey neutrons that go through more than one blade) is given by the expression:

$$\tan\xi \simeq \frac{R_M}{(R_M - R_{SE})}\tan 2\phi \qquad (23)$$

From here, ξ = 9.6°, and thus, the minimum thickness of the gadolinium layer is $t \simeq 30$ μm.

4 Conclusions

This work reports on the conceptual design for a radial collimator to be installed in a neutron backscattering instrument. A general design concept is developed, by which the focal lines and focal points that define every collimation channel serve in turn to parametrize the dimensional features of the collimator (inner and outer radius, slit/channel angle) and figures of merit that provide information about the performance of the

collimator (transmission, background reduction, detector impact) in the forward and backscattering neutron pathways.

The general expressions obtained were eventually applied to MIRACLES, the time-of-flight backscattering spectrometer at the European Spallation Source. For MIRACLES, the focal width has been determined by the sample bore of the cryostat dedicated to the instrument; the slit aperture has been defined by the solid angle covered by the tube detectors; and the inner radius has been determined by the position of the detectors, as well as by mechanical design constraints. Finally, an estimation of the neutron capturing layer that coats the collimation blades has been estimated considering the grazing incidence angles at which neutrons scattered by the sample environment reach the collimation channels.

This research is partially funded by the Next Generation EU–Recovery and Resilience Facility (RRF). We would like to express our gratitude to Gorka Mujika (ESS-Bilbao); his continued encouragement along the whole research process, from the initial conception of the idea to the draft writing, has been determinant for the successful accomplishment of this work.

References

1. E. Mamontov, K. W. Herwig, Rev. Sci. Instrum. **82**, 085109 (2011)
2. K. H. Andersen, D. Martín y Marero, M. J. Barlow, Appl. Phys. A Mater. Sci. Process. **74**, (2002)
3. M. B. Stone, J. L. Niedziela, M. A. Overbay, D. L. Abernathy, EPJ Web Conf. **83**, 03014 (2015)
4. M. B. Stone, J. L. Niedziela, M. J. Loguillo, M. A. Overbay, D. L. Abernathy, Rev. Sci. Instrum. **85**, 085101 (2014)
5. J. R. D. Copley J. C. Cook, Nucl. Inst. Methods Phys. Res. A **345**, 313 (1994)
6. J. Bouillot, J. Torregrossa, Rev. Phys. Appliquée **19**, 799 (1984)
7. M. Nakamura, W. Kambara, K. Iida, R. Kajimoto, K. Kamazawa, K. Ikeuchi, M. Ishikado, K. Aoyama, Phys. B Condens. Matter **551**, 480 (2018)
8. K. H. Andersen *et al.* Nucl. Instruments Methods Phys. Res. Sect. A Accel. Spectrometers, Detect. Assoc. Equip. **957**, 163402 (2020)
9. N. Tsapatsaris, R. E. Lechner, M. Markó, H. N. Bordallo, Rev. Sci. Instrum. **87**, 085118 (2016)
10. M. Yonemura, K. Mori, T. Kamiyama, T. Fukunaga, S. Torii, M. Nagao, Y. Ishikawa, Y. Onodera, D. S. Adipranoto, H. Arai, Y. Uchimoto, Z. Ogumi, in *J. Phys. Conf. Ser.* (Institute of Physics Publishing, 2014)
11. I. P. Orench, J. F. Clergeau, S. Martínez, M. Olmos, O. Fabelo, J. Campo, J. Phys. Conf. Ser. **549**, 012003 (2014)
12. D. L. Abernathy, M. B. Stone, M. J. Loguillo, M. S. Lucas, O. Delaire, X. Tang, J. Y. Y. Lin, B. Fultz, Rev. Sci. Instrum. **83**, 015114 (2012)
13. K. Lefmann, K. Nielsen, Neutron News **10**, 20 (1999)